NUMERICAL SIMULATION OF HEAT TRANSFER BY MIXED CONVECTION IN HORIZONTAL FINNED CHANNELS

Paulo Laranjeira da Cunha Lage, paulo@peq.coppe.ufrj.br
Gabriel Gonçalves da Silva Ferreira, ggsferreira@gmail.com
Fabio Pereira dos Santos, fpereira@peq.coppe.ufrj.br
Programa de Engenharia Química – COPPE, Universidade Federal do Rio de Janeiro, PO Box 68502, Rio de Janeiro, RJ 21941 972, Brazil

Luiz Fernando Lopes Rodrigues Silva, lflopes@eq.ufrj.br
Escola de Química – Universidade Federal do Rio de Janeiro, Centro de Tecnologia, Av. Athos da Silveira Ramos, 149, Rio de Janeiro, RJ 21941 909, Brazil

Abstract. *Fins are extended surfaces often used to increase the heat transfer rate from a solid surface to a fluid by increasing the interfacial area and promoting a better mixing of the fluid. However, to accomplish this objective efficiently, these surfaces must be composed of high thermal conductivity materials and, depending on the type of the flow, different geometries must be applied to achieve the optimal design. In this work, a numerical model for the mixed convection heat transfer with turbulent flow in a horizontal finned channel was evaluated. The modeled geometry consisted of a rectangular channel with longitudinal plate fins heated from below by a heated surface. The mathematical model consisted of the Reynolds-averaged Navier-Stokes and thermal energy equations coupled to the shear stress transport (SST) turbulence model. For the heat transfer evaluation, the SST model requires a high level of discretization of the boundary layer. Thus, fine hexaedrical meshes were constructed. The effect of conjugate heat transfer was taken in account, but the radiation heat transfer was neglected. Numerical results were obtained for different temperatures of the heated surface and the values of the mean convection heat transfer coefficient were evaluated and compared with experimental data to validate the model. The effect of conjugation and buoyancy on heat transfer were evaluated.*

Keywords: *conjugate heat transfer, mixed convection, CFD, rectangular plate fins*

1. INTRODUCTION

The heat transfer rate between a solid surface and a fluid can be increased installing fins which will enlarge the interfacial exchange area and may affect the flow pattern (Incropera *et al.*, 2011). In fact, the flow regime is largely affected by the geometry of the fins and its spacial configuration. The mixed convection flow regime is usually found on many fin configurations as, for instance, nuclear reactors cooling (Bairi, 2008) and electronic components (Anandan and Ramalingam, 2008), among others. As a matter of fact, the knowledge of the physical behavior and the application of theoretical or empirical models are important to predict the performance of these systems. For instance, in electronic cooling systems, the natural buoyancy of heated air allows designers to avoid active cooling, increasing reliability and decreasing costs.

Several works dealing with the experimental analysis of the heat transfer using fins under natural and forced convection flow regimes can be found in the literature (Islam *et al.*, 2009; Dogan and Sivrioglu, 2010; Elshafei, 2010). In general, these works intended to evaluate the thermal performance of heat sinks using fins over different flow regimes and configurations.

Many authors have also evaluated the thermal performance of different types of fins for the natural convection flow regime using CFD codes. Yu and Joshi (2002) used computational modeling and thermal measurements to investigate the effects of natural convection, conduction and radiation using pin fins in a enclosed cavity. Since the existing correlations for natural convection heat transfer in free space showed large deviations from their measurements, the effects of flow confinement were found prominent. Rao *et al.* (2006) performed numerical simulations to evaluate the effect of natural convection and radiation considering the conjugate heat transfer problem for natural convection in a horizontal heat sink with plate fins. They studied it's effectiveness for different values of fin heights, emissivities, base temperature, fin number and spacing. Their results were in good agreement with the experimental data available in literature (Rao and Venkateshan, 1996). Bairi (2008) studied the classical problem of natural convection in an enclosed cavity at high Rayleight numbers using the RNG-$\kappa\epsilon$ turbulence model. The simulation and experimental results were compared, showing an overall agreement. Haldar (2010) studied the laminar natural convection in a cylindrical pin element attached to a base plate. He developed a correlation to predict the heat transfer rate based on the fin diameter to length ratio and the Grashoff number.

There are also several works numerically evaluating the forced convection heat transfer in fin arrays. Soodphakdee *et al.* (2001) performed several CFD simulations to analyze the performance of round, elliptical and plate fins on staggered

and in-line configurations. They found that, in general, the staggered plate fin geometry has the highest heat transfer rate for a given combination of pressure gradient and flow rate. Sahiti *et al.* (2007) developed a simple and practical procedure for selection and optimization of pin fins for electronic cooling. They found that the elliptical shape has a better performance compared with the circular shape. Mitre *et al.* (2010) analyzed numerically the heat transfer in pin-fin channels with aligned and staggered arrangements for forced convection turbulent flow regime. The CFD results agreed with experimental data and the predictions using the correlations of Grimison (1938), Zukauskas (1972) and Chyu *et al.* (1999).

Ozsunar *et al.* (2002) evaluated experimentally the mixed convection heat transfer in rectangular channels for horizontal and inclined configurations. They presented experimental results for the Nusselt number based on the Grashoff and Reynolds numbers of the flow, the channel aspect ratio and it's inclination. Al-Sarkhi *et al.* (2003) studied numerically the influence of combined free and forced convection in a vertical shrouded channel with plate fins. They studied the effect of Reynolds and Rayleight numbers and the channel height in the thermal performance of the heat sink. Baskaya *et al.* (2005) investigated experimentally the mixed convection heat transfer from an array of discrete heat sources inside a rectangular channel for different values of the Reynolds and Grashoff numbers. Kobus and Oshio (2005) carried out a theoretical and experimental study to investigate the influence of thermal radiation on the thermal performance of a pin fin array heat sink under mixed convection flow regime. The validation of a theoretical model capable of predicting the influence of thermal performance of a pin fin array heat sink was performed. Yang *et al.* (2010) studied numerically the mixed convection heat transfer in an inclined parallel-plate channel with rectangular fins. They evaluated the effects of the Reynolds and Grashoff numbers in the optimum fin aspect ratio.

Dogan and Sivrioglu (2010) experimentally investigated the effect of fin spacing and fin height on the heat transfer rate for mixed convection flow in finned channels. They found that the heat transfer rate increases first with fin spacing, reaches a maximum value and then decreases. When the fin spacing is smaller than a specific value, the flow resistance increases due to the intersection of the boundary layers. On the other hand, larger fin spacing results on a smaller number of fins for a fixed base area, decreasing the heat transfer rate. They also concluded that the optimum fin spacing depends mainly on the temperature difference between the inlet fluid and the base temperature.

The aim of the present work is to numerically analyze the conjugate heat transfer in a rectangular channel with longitudinal rectangular plate fins in the mixed convection turbulent flow regime. The simulated geometry was chosen to be the one experimentally evaluated by Dogan and Sivrioglu (2010) in their experimental study. Comparison between CFD and their experimental results was made to validate the numerical model. The conjugate heat transfer and buoyancy effects on the total heat transfer rate were also evaluated.

2. METHODOLOGY

2.1 Fluid model

The flow was considered to be compressible, non-isothermal and three dimensional. The Reynolds-averaged Navier-Stokes (RANS) equations are given by

$$\frac{\partial \rho}{\partial t} + \nabla \cdot (\rho \mathbf{U}) = 0 \tag{1}$$

$$\frac{\partial (\rho \mathbf{U})}{\partial t} + \nabla \cdot \{\rho\, \mathbf{U} \otimes \mathbf{U}\} - \nabla \cdot (\mu_{eff} \nabla \mathbf{U}) = -\nabla p' + \nabla \cdot [\mu_{eff} (\nabla \mathbf{U})^T] + (\rho - \rho_{ref})\mathbf{g} \tag{2}$$

where the effective viscosity is defined by $\mu_{eff} = \mu + \mu_t$ and p' is a modified pressure, given by

$$p' = p - p_{ref} + \frac{2}{3}\left[\rho\kappa + \mu_{eff}(\nabla \cdot \mathbf{U})\right] \tag{3}$$

where $\mathbf{r}$ is the position in the fluid domain that the pressure is being calculated, $\mathbf{r_{ref}}$ is a reference location, p_{ref} is the reference pressure, which is defined by $p_{ref} = \rho_{ref}\mathbf{g} \cdot (\mathbf{r} - \mathbf{r_{ref}})$, ρ_{ref} is the fluid density and κ is the turbulent kinetic energy. The last term in the right-hand side of eq. 3 is not considered in the *ANSYS CFX* implementation.

The Reynolds-averaged thermal energy equation is

$$\frac{\partial (\rho h)}{\partial t} + \nabla \cdot (\rho h \mathbf{U}) = \nabla \cdot \left[\left(\frac{\lambda}{C_P} + \frac{\mu_t}{Pr_t} \right) \nabla h) \right] \tag{4}$$

In eq. 4, viscous dissipation and compressibility effects were neglected, which is adequate for low Mach number flows. The SST turbulence model (Menter, 1994; Menter *et al.*, 2002) was employed in this work. This turbulence model is indicated for calculation of skin friction and heat transfer at solid surfaces. It reduces itself to the $\kappa - \omega$ model near the wall and the $\kappa - \epsilon$ far from the wall. The SST turbulence model equations are given by

$$\frac{\partial (\rho \kappa)}{\partial t} + \nabla \cdot (\rho \kappa \mathbf{U}) = \nabla \cdot [(\mu + \mu_t \sigma_{\kappa 3}) \nabla \kappa] + P_\kappa + \beta^* \rho \omega \kappa + P_{\kappa B} \tag{5}$$

$$\frac{\partial(\rho\omega)}{\partial t} + \nabla\cdot(\rho\omega\mathbf{U}) = \nabla\cdot[(\mu + \mu_t\sigma_{\omega 3})\nabla\omega] + 2(1-F_1)\rho\sigma_{\omega 2}\frac{1}{\omega}\nabla\kappa\cdot\nabla\omega + \frac{\alpha_3\omega}{\kappa}P_\kappa - \beta_3\rho\omega^2 + P_{\omega B} \tag{6}$$

where P_κ is the shear production of turbulence defined by

$$P_\kappa = \min(\mathbf{T}_t : \nabla\mathbf{U}, 10\rho\epsilon) \tag{7}$$

With $\epsilon = \beta^*\omega\kappa$ and the Reynolds stress tensor is given by

$$\mathbf{T}_t = \mu_t[\nabla\mathbf{U} + (\nabla\mathbf{U})^T] - \frac{2}{3}\mathbf{I}(\rho\kappa + \mu_t\nabla\cdot\mathbf{U}) \tag{8}$$

All the model constants are calculated by combining the $\kappa-\epsilon$ and the $\kappa-\omega$ models using a blending function $\alpha_3 = \alpha_1 F_1 + \alpha_2(1-F_1)$ where α_1 and α_2 are the parameters from $\kappa-\omega$ and $\kappa-\epsilon$ models, respectively. The value of these parameters are: $\beta^* = 0.09$, $\alpha_1 = 5/9$, $\beta_1 = 3/40$, $\sigma_{\omega 1} = 0.5$, $\sigma_{\kappa 1} = 0.5$, $\alpha_2 = 0.44$, $\beta_2 = 0.0828$, $\sigma_{\kappa 2} = 1$ and $\sigma_{\omega 2} = 0.856$.

The blending function F_1 is defined by

$$F_1 = \tanh\left(\left\{\min\left[\max\left(\frac{\sqrt{\kappa}}{\beta^*\omega y}, \frac{500\nu}{y^2\omega}\right), \frac{4\rho\sigma_{\omega 2}\kappa}{CD_{\kappa\omega}y^2}\right]\right\}^4\right) \tag{9}$$

where y is the distance to the nearest wall and $CD_{\kappa\omega}$ is given by

$$CD_{\kappa\omega} = \max\left(2\rho\frac{\sigma_{\omega 2}}{\omega}\nabla\kappa\cdot\nabla\omega, 10^{-10}\right) \tag{10}$$

The turbulent eddy viscosity is defined as

$$\nu_t = \frac{a_1\kappa}{\max(a_1\omega, SF_2)} \tag{11}$$

where $a_1 = 0.31$, S is the invariant measure of the strain rate given by $S = \sqrt{2D:D}$ and F_2 is a second blending function defined by

$$F_2 = \tanh\left\{\left[\max\left(\frac{2\sqrt{\kappa}}{\beta^*\omega y}, \frac{500\nu}{y^2\omega}\right)\right]^2\right\} \tag{12}$$

The additional production term due to buoyancy in the κ–equation is given by

$$P_{\kappa B} = -\frac{\mu_t}{\rho}\mathbf{g}\cdot\nabla\rho \tag{13}$$

and additional buoyancy term in the ω – equation is given by

$$P_{\omega B} = \frac{\omega}{\kappa}[(\alpha+1)C_3\max(P_{\kappa B}, 0) - P_{\kappa B})] \tag{14}$$

the term C_3 is the dissipation coefficient, which was set to 1.

The formulation of the flow near the wall switches automatically from scalable wall-functions to low-Re formulations depending on the mesh refinement. The $\kappa-\omega$ model of Wilcox has an analytical expression for ω in the viscous sublayer, which can be applied for this goal. The current formulation blends the near-wall ω value given by the logarithmic law with a low-Re near wall formulation. In this formulation the flux for the κ equation is artificially set to zero. Thus, the flux in the momentum equation is calculated by the velocity profile, and it is given by

$$F_U = -\rho u_\tau u^* \tag{15}$$

with

$$u^* = \sqrt[4]{\left(\sqrt{\frac{\mu}{\rho}\left|\frac{\Delta U}{\Delta y}\right|}\right)^4 + (\sqrt{a_1\kappa})^4} \tag{16}$$

$$u_\tau = \sqrt[4]{(u_\tau^{vis})^4 + (u_\tau^{log})^4} \tag{17}$$

where

$$u_\tau^{vis} = \sqrt{\frac{\mu}{\rho}\left|\frac{\Delta U}{\Delta y}\right|} \tag{18}$$

$$u_\tau^{log} = \frac{U}{1/\kappa \log(y^+) + C} \tag{19}$$

In the ω-equation an algebraic equation is specified instead of the flux. This expression results from the blending of the analytical expression for ω in the logarithmic region, ω_l, which is given by

$$\omega_l = \frac{u^*}{a_1 \kappa y} = \frac{1}{a_1 \kappa \nu} \frac{{u^*}^2}{y^+} \tag{20}$$

and the corresponding equation ω equation for the viscous sublayer, ω_s, given by

$$\omega_s = \frac{6\nu}{\beta(\Delta y)^2} \tag{21}$$

with Δy being the distance between the first and the second mesh point. The near wall ω value is finally calculated by

$$\omega_{wall} = \omega_s \sqrt{1 + \left(\frac{\omega_l}{\omega_s}\right)^2} \tag{22}$$

The thermal boundary layer is modeled using the thermal law-of-the-wall function of Kader (1981). Using the same assumptions in modeling the flow near the wall, the heat flux at the wall, q_w, is given by

$$q_w = \frac{\rho c_p u^* (T_w - T_f)}{T^+} \tag{23}$$

where T^+ is the dimensionless temperature whose profile is given by:

$$T^+ = \mathrm{Pr} y^* \mathrm{e}^{(-\Gamma)} + [2.12 \ln(y^*) + \beta] \mathrm{e}^{(-\Gamma)} \tag{24}$$

and β and Γ are dimensionless parameters given by:

$$\beta = \left(3.85 \mathrm{Pr}^{1/3} - 1.3\right)^2 + 2.12 \ln(\mathrm{Pr}) \tag{25}$$

and

$$\Gamma = \frac{0.01 (y^* \mathrm{Pr})^4}{1 + 5 y^* \mathrm{Pr}^3} \tag{26}$$

where Pr is the Prandtl's number of the fluid.

2.2 Solid model

Conjugate heat transfer was taken in account, so the individual temperature field of each fin was calculated. The energy equation for a static solid domain without volumetric heat sources is given by

$$\rho_s \frac{\partial (C_{Ps} T)}{\partial t} - \nabla \cdot (\lambda_s \nabla T) = 0 \tag{27}$$

where ρ_s, λ_s and C_{Ps} are the density, thermal conductivity and specific heat of the solid material.

2.3 Fluid and solid properties

The ideal gas equation of state was used for calculating the air density ρ. Empirical correlations for the other fluid and solid thermo-physical properties were developed based on experimental literature data for air and aluminium (Incropera *et al.*, 2011). These empirical expressions were implemented in *ANSYS CFX 12.1*. The air specific heat was given by $C_P = 1000(1.0331 - 0.0624\theta + 0.036\theta^2)$ J/kgK, the air thermal conductivity was calculated by $\lambda = 0.026227\theta^{0.881091}$ W/mK and the air dynamic viscosity was calculated by $\mu = 1.8431 \times 10^{-5}\, \theta^{0.776953}$ Ns/m^2. The solid properties were given by $C_{Ps} = 765 + 138\theta$ J/kgK, $\lambda_s = \min(9 \max(\theta, 1) + 228, 240)$ W/mK and $\rho_s = 2702$ kg/m^3. In these formulations the dimensionless temperature, θ, was defined by $\theta = T(\mathrm{K})/(300\mathrm{K})$.

3. NUMERICAL PROCEDURE

The experimental setup used by Dogan and Sivrioglu (2010) consisted of a filter, a nozzle, the test section, a damping chamber, a diffuser, a flow control valve and an AC fan. The valve and the fan were responsible for maintaining a nearly constant air velocity at the channel between $0.15 < w_{in} < 0.16$ m/s at the inlet conditions, giving a Reynolds number around $Re = 1500$. The test section consisted of a rectangular channel with height $H = 0.1$ m, width $W =$

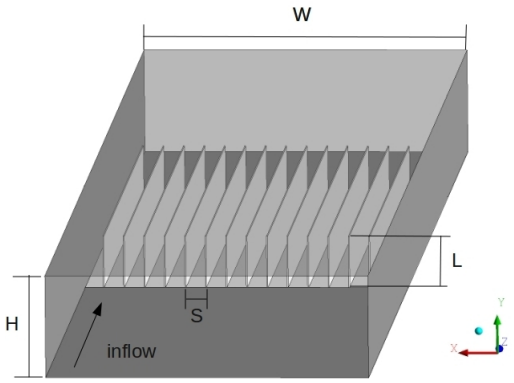

Figure 1. The modeled geometry.

0.3 m and a length $L = 1.5$ m, with a heated section located 0.3 m after its entrance. This section consisted of a $5 \times 300 \times 600$ mm copper plate with aluminium longitudinal fins of 1 mm thickness and 0.3 m length. The experimental work of Dogan and Sivrioglu (2010) tested different values of fin heights ($l = 0.25H, 0.5H, 0.75H$) and fin spacing ($S = 0.04H, 0.08H, 0.12H, 0.18H$) and evaluated the influence of these parameters in the total heat transfer rate Q. For the current work, an array of 15 ($S = 0.18H$) aluminium fins with $l/H = 0.5$ was reproduced for the simulations and it is shown in Fig. 1.

In order to evaluate the importance of conjugate heat transfer and buoyancy effects on the heat transfer rate, three different models were applied. Model 1 takes in account the buoyancy effects in the flow and the heat conduction in the solid domain, solving the heat conduction equation in the fins. Model 2 neglects the conjugate heat transfer effect by assuming that the base temperature is valid over all fin surface, that is, fin efficiency is 100%. This model still includes buoyancy effects. On the other hand, model 3 still takes into account the conjugate heat transfer but it neglects the buoyancy force.

3.1 Boundary conditions

Dogan and Sivrioglu (2010) performed experiments varying the base temperature of the heat sink and the fin spacing and channel height for a controlled mass flow rate. Therefore, a constant air mass flow rate, $W_{in} = 5.51$ kg/s, with the velocity normal to the inlet channel cross section was setas the boundary condition at the entrance of the channel, with a turbulence intensity of 5%. The inlet thermal boundary condition was set to a fixed temperature, $T_{inlet} = 25^o$C.

At the channel outlet, a boundary condition called *opening* by *CFX* was applied. This type of boundary condition specifies the pressure level at the outlet surface and the velocity is calculated, either for inflow or outflow. The velocity was assumed to be normal to this surface. A constant temperature boundary condition was set to the heated plate and fins base. In order to test the applied modeling, three different values of base temperature ($T_b = 43.4$,50.9 and 56.6^oC) used by Dogan and Sivrioglu (2010) were considered in this work.

The conjugate heat transfer effects were taken in account in model 1. Thus, a heat flux conservation was assumed at the fluid-fin interfaces. However, for the model 2, a constant temperature boundary condition was set to base and fin surface. All other solid walls were considered adiabatic. The no-slip boundary condition was set to all solid walls.

3.2 Mesh

Three meshes consisting only of hexaedrical elements were built in order to achieve mesh convergence. The coarser mesh is shown at Fig. 2. For accurate heat transfer calculations with the SST turbulence model, a value of y^+ around 1 at the wall and at least 10 nodes at the boundary layer discretization are necessary. In order to check mesh convergence, the total heat transfer rate at the heated surface and the temperature profile at some regions of the fluid domain were monitored after obtaining the results given by the model 1. Table 1 shows the number of elements of the used meshes for the fluid and solid domains.

Table 1. Number of elements of the built meshes (model 1).

Mesh size	Fluid nodes	Fluid nodes ratio	Solid nodes	Solid nodes ratio	Total nodes	Total nodes ratio
1	1578375	1	99990	1	1678365	1
2	3020360	1.9	284310	2.8	3304670	2.0
3	6229430	3.9	557280	5.6	6786710	4.0

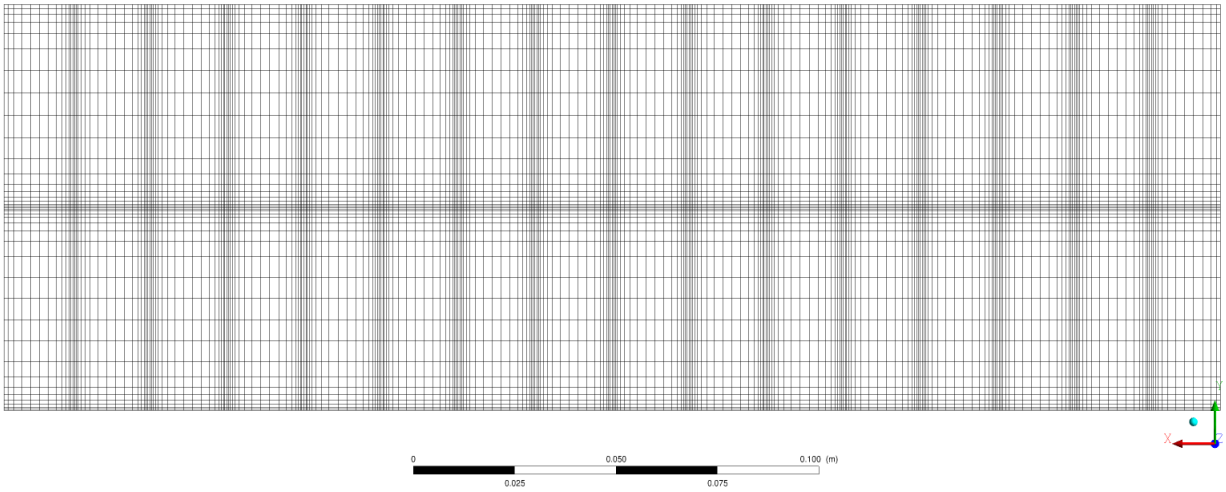

Figure 2. Fluid domain of the coarsest mesh (size 1).

Table 2. CFD Results for the total heat transfer rate (model 1).

Case	ΔT (K)	Q_{CFD}(W)	Q_{exp}(W)	error (%)
1	18.4	50.4±0.1	45.3	11.2
2	25.9	76.3±0.3	72.6	5.0
3	31.6	97.4±0.4	89.1	9.3

3.3 Numerical Solution

The computations were performed in single precision using *ANSYS CFX 12.1*, which uses a coupled solver for the hidrodinamic equations (RANS) as a single system. In transient simulations, the solver uses a a fully implicit discretization of the equations for a given time step. For steady-state problems, the time-step behaves like an accelerator parameter to guide the solver in a physically based manner to the solution. This time step (fluid time scale) is calculated based on physical parameters of the flow, like the dimensions of the geometry and averaged velocity values at the domain boundaries. Further information about the solver methodology and capabilities is found at *ANSYS CFX-Solver Theory Guide* The convergence was achieved when the maximum normalized residual value of all discretized equations was smaller than 10^{-5}.

4. RESULTS AND DISCUSSION

Simulations with three different heated surface temperatures, as shown in Table 2, were performed. The total heat transfer rate at the heated surface (Table 3) and the temperature profile at the line $x/W = 0.5$, $y/H = 0.75$, above the fins in the fluid domain (Figure 3) were monitored to verify the mesh convergence. The average and maximum values of y^+ at the heated surface are presented in Table 3 for the case 3 (model 1), which has the largest heated surface temperature.

These results show that there is no significant difference between the heat transfer rate and temperature profiles obtained using the meshes size 2 and 3. Therefore, mesh 2 was considered to be adequate for the numerical simulations.

Table 2 contains the simulated results for the total heat transfer rate of the three cases analyzed, (Q_{CFD}), as well as the experimental data from Dogan and Sivrioglu (2010) (Q_{exp}). The relative error between these values were calculated and are also shown in Table 2. The prediction errors vary from 5–11%. It can be said that this is a good agreement with the experimental data because the experimental error evaluated by Dogan and Sivrioglu (2010) for the heat transfer coefficients (Nusselt numbers) was 6%. The error associated to the CFD results were calculated based on the difference between the results obtained by using the meshes size 3 and 2.

Table 3. Mesh convergence and y^+ data at the heated plate and fin surface for the case 3 (model 1).

Mesh size	y^+_{ave}	$\max(y^+)$	Q_{CFD}(W)	$\Delta Q_{CFD}\%$
1	0.65	1.84	97.77	0
2	0.36	1.18	97.40	0.38
3	0.14	0.67	96.97	0.82

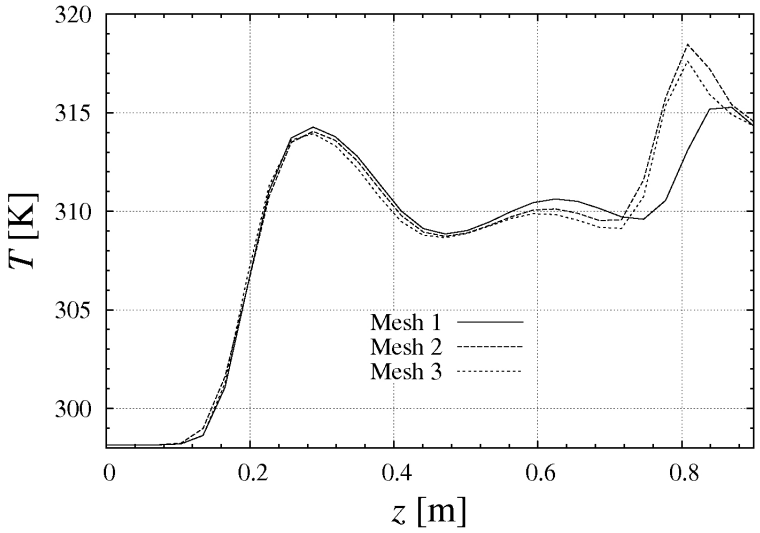

Figure 3. Temperature profile at $x = 0.5W$, $y = 0.75H$. The plane $z = 0$ is located at the beginning of the heated section.

Table 4 shows a comparison between the results for the heat transfer rate provided by models 1, 2 and 3 ($Q_{CFD,i}$ for model i). It can be seen that the errors related to the neglect of the heat conduction in the fins are around 3%. They agree to the fin efficiency estimate by steady-state one-dimensional conduction whose values were around 97 – 98%. The comparison between the heat transfer rates simulated by models 1 and 3 shows the importance of natural convection in the present problem. If this is considered a forced convection problem (model 3), the heat transfer rate is unpredicted by as much as 38%. Therefore, it is quite clear that this is a mixed convection problem. The effect of buoyancy on the heat transfer rate occurs by the generation of a secondary flow in the cross section area of the channel, as can be seen in Figure 4. This secondary flow causes an additional fluid mixing and large differences in the temperature fields simulated by models 1 and 3, as can be seen in Figures 5(a) and 5(b), respectively. It can also be seen in Figure 5(a) that the temperature field at the fin surface is almost constant, except at the beginning of the test section, which also supports the application of model 2 for heat transfer calculations.

5. CONCLUSION

A numerical model was used to predict the conjugate heat transfer in horizontal finned channels for mixed convection turbulent flows. The model consisted of the Reynolds-averaged Navier-Stokes equation coupled to the Reynolds-averaged thermal energy equation and the shear stress transport (SST) turbulence model. Validation of the model was made by comparing the CFD results with experimental data from Dogan and Sivrioglu (2010). The conjugate heat transfer effects were evaluated and they were responsible for a 3% reduction in the heat transfer rate for the cases analyzed. It was verified that buoyancy appreciably affects the heat transfer rate, but the effect of forced convection is still relevant. Therefore, the problems analysed belong to the mixed convection regime.

6. REFERENCES

Al-Sarkhi, A., Abu-Nada, E., Akash, B.A. and Jaber, J.O., 2003. "Numerical investigation of shrouded fin array under combined free and forced convection". *International Communications in Heat and Mass Transfer*, Vol. 30, No. 3, pp. 435–444.

Anandan, S.S. and Ramalingam, V., 2008. "Thermal management of electronics: A review of literature". *Thermal Science*, Vol. 12, No. 2, pp. 5–26.

Table 4. Evaluation of conjugate heat transfer and buoyancy effects for different temperatures.

Case	$Q_{CFD,1}$ (W)	$Q_{CFD,2}$ (W)	$\left\lvert\frac{Q_{CFD,1}-Q_{CFD,2}}{Q_{CFD,1}}\right\rvert$ (%)	$Q_{CFD,3}$ (W)	$\left\lvert\frac{Q_{CFD,1}-Q_{CFD,3}}{Q_{CFD,1}}\right\rvert$ (%)
1	50.4	51.9	3.0	35.2	30.1
2	76.3	78.6	3.0	49.3	35.4
3	97.4	100.2	2.9	60.1	38.3

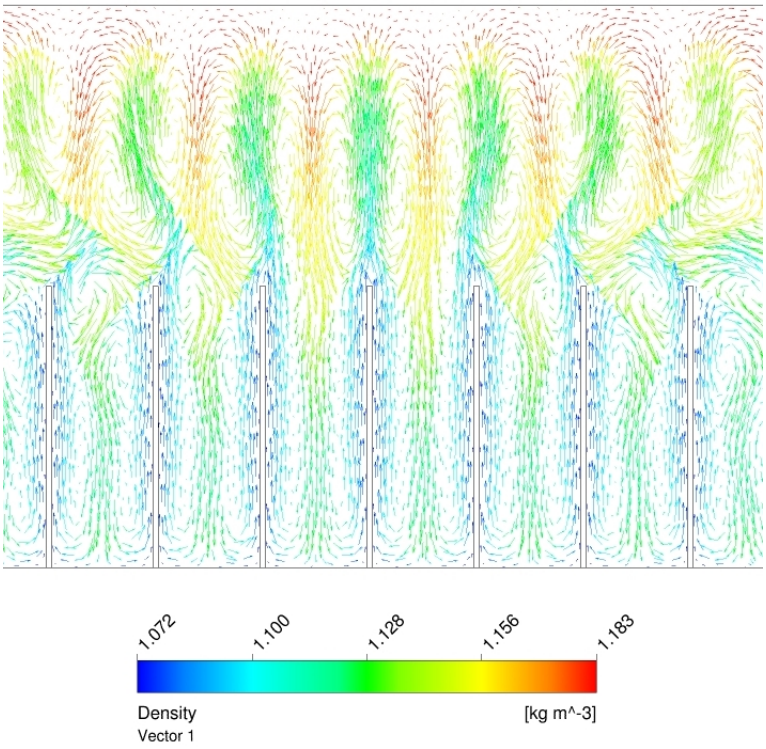

Figure 4. Secondary flow pattern and air density profile in the middle of the finned section.

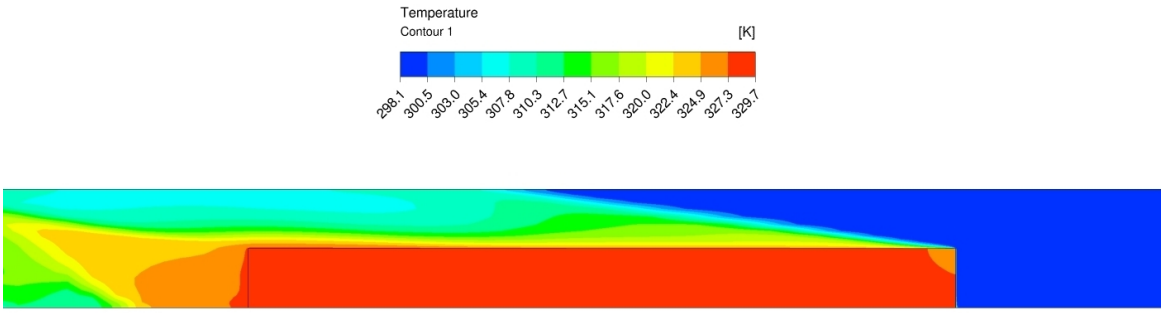

(a)

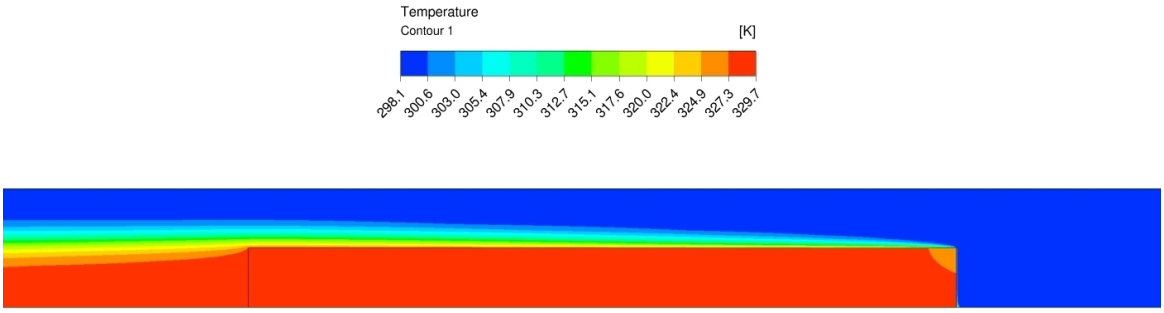

(b)

Figure 5. Temperature profile at the test section for the plane $x = 0.5W$, case 3: (a) model 1 and (b) model 3.

Bairi, A., 2008. "Nusselt-Rayleight correlations for design of industrial elements: Experimental and numerical investigation of natural convection in tilted square air filled enclosures". *Energy Conversion and Management*, Vol. 49, pp. 771–782.

Baskaya, S., Erturhan, U. and Sivrioglu, M., 2005. "Experimental investigation of mixed convection from an array of discrete heat sources at the bottom of a horizontal channel". *Heat Mass Transfer*, Vol. 42, pp. 56–63.

Chyu, M., Hsing, Y.C. and Shih, T.I.P., 1999. "Heat transfer contributions of pins and endwall in pin-fin arrays: Effects of thermal boundary condition modeling". *J Turbomachinery*, Vol. 121, pp. 257–263.

Dogan, M. and Sivrioglu, M., 2010. "Experimental investigation of mixed convection heat transfer from longitudinal fins in a horizontal rectangular channel". *International Journal of Heat and Mass Transfer*, Vol. 53, pp. 2149–2158.

Elshafei, E.A.M., 2010. "Natural convection heat transfer from a heat sink with hollow/perforated circular pin fins". *Energy*, Vol. 35, pp. 2870–2877.

Grimison, E.D., 1938. "Correlation and utilization of new data on flow resistance and heat transfer for crossflow of gases over tube banks". *Transactions of the ASME*, Vol. 60, pp. 384–386.

Haldar, S.C., 2010. "Natural convection about a cylindrical pin element on a horizontal plate". *International Journal Thermal Sciences*, Vol. 49, pp. 1977–1983.

Incropera, F.P., DeWitt, D.P., Bergman, T.L. and Lavine, A.S., 2011. *Fundamentals of Heat and Mass Transfer*. John Wiley & Sons, Inc., 7th edition.

Islam, M.D., Oyakawa, K., Yaga, M. and Kubo, I., 2009. "The influence of channel height on heat transfer enchancement of a co-angular type rectangular finned surface in narrow channel". *International Journal of Thermal Sciences*, Vol. 48, pp. 1639–1648.

Kader, B.A., 1981. "Temperature and concentration profiles in fully turbulent boundary layers". *International Journal of Heat and Mass Transfer*, Vol. 24 (9), pp. 1541–1544.

Kobus, C.J. and Oshio, T., 2005. "Predictiong the thermal performance characteristics of staggered vertical pin fin array heat sinks under combined mode radiation and mixed convection with impinging flow". *Heat and Mass Transfer*, Vol. 48, pp. 2684–2696.

Menter, F.R., 1994. "Two equation eddy-viscocity turbulence models for engineering applications". *AIAA J*, Vol. 32, No. 8, pp. 1598–1605.

Menter, F.R., Vieser, W. and Esch, T., 2002. "Heat transfer predicitions using advanced two-equation turbulence models". *CFX-Validation Report*, Vol. CFX-VAL10/0602.

Mitre, J.F., Santana, L.M., Damian, R.B., Su, J. and Lage, P.L.C., 2010. "Numerical study of turbulent heat transfer in 3D pin-fin channels: Validation of a quick procedure to estimate mean values in quasi-periodic flows". *Applied Thermal Engineering*, Vol. 30, pp. 2796–2803.

Ozsunar, A., Baskaya, S. and Sivrioglu, M., 2002. "Experimental investigation of mixed convection heat transfer on a horizontal and inclined rectangular channel". *Heat and Mass Transfer*, Vol. 38, pp. 271–278.

Rao, R. and Venkateshan, S.P., 1996. "Experimental study of free convection and radiation in horizontal fin arrays". *International Journal of Heat and Mass Transfer*, Vol. 39, pp. 779–789.

Rao, V.D., Naidu, S.V., Rao, B.G. and Sharma, K.V., 2006. "Heat transfer from a horizontal fin array by natural convection and radiation – A conjugate analysis". *International Journal of Heat and Mass Transfer*, Vol. 49, pp. 3379–3391.

Sahiti, N., Durst, F. and Geremia, P., 2007. "Selection and optimization od pin cross-sections for electronics cooling". *Applied Thermal Engineering*, Vol. 27, pp. 111–119.

Soodphakdee, D., Behnia, M. and Copeland, D.W., 2001. "A comparison of fin geometries for heatsinks in laminar forced convection: Part 1 - Round, elliptical and plate fins in staggered and in-line configurations". *The International Journal of Microcircuits and Electronic Packaging*, Vol. 24, No. 1, pp. 68–76.

Yang, M., Yeh, R. and Hwang, J., 2010. "Mixed convective cooling of a fin in a channel". *International Journal of Heat and Mass Transfer*, Vol. 53, pp. 760–771.

Yu, E. and Joshi, Y., 2002. "Heat transfer enhancement from enclosed discrete components using pin-fin heat sinks". *International Journal of Heat and Mass Transfer*, Vol. 45, pp. 4957–4966.

Zukauskas, A., 1972. "Heat transfer from tubes in crossflow". *Advances in Heat Transfer*, Vol. 8, pp. 93–160.